$R_{sl}$ = 0.0670 (0.0098), was obtained for the combination of the 19-ch EEG and a prior with R = 18. However, in the first step, the average (SD) of $R_{sl}$ was only 0.0188 (0.0118) when the prior was not available even if the number of EEG sensors was the maximum, 64. Therefore, R = 18 with 19 EEG sensors led to markedly higher performance. Fig. 7B shows the results for $R_s$. Two-way ANOVA revealed significant effects of the resolution of prior information [$F(2, 4499) = 21{,}958.09$, $p<0.05$] and the number of EEG sensors [$F(2, 4499) = 49.62$, $p<0.05$], but interaction between these factors was not significant [$F(4, 4499) = 0.15$, $p = 0.965$]. Just like the $R_{sl}$ case, the correlation became lower as the resolution worsened and as the number of EEG sensors decreased (multiple comparison, $p<0.05$). The lowest correlation, $R_s = 0.080$ (0.0104), was obtained for the combination of the 19-ch EEG and prior with R = 18. However, in the first step, the average (SD) of $R_s$ was only 0.0389 (0.0178) when the prior was not available even if the number of EEG sensors was the maximum, 64. Therefore, R = 18 with 19 EEG sensors was far better. Fig. 7C illustrates the results of the RMSE. Two-way ANOVA revealed significant effects of the resolution of prior information [$F(2, 4499) = 4574.81$, $p<0.05$] and the number of EEG sensors [$F(2, 4499) = 139.82$, $p<0.05$] and a significant interaction between these factors [$F(4, 4499) = 16.7$, $p<0.05$]. RMSE became larger as the resolution of the prior worsened and as the number of EEG sensors decreased (multiple comparison, $p<0.05$). The largest RMSE was $4.3367\times10^{-11}$ ($2.6579\times10^{-14}$) [Am] for the combination of 19-ch EEG and prior with R = 18. However, considering that the average (SD) of RMSE was $4.3575\times10^{-11}$ ($3.4765\times10^{-14}$) [Am] when no prior was available, using the prior with R = 18 produced markedly better performance. Taken together, the performance of VBMEG worsened as the resolution of the prior became lower and as the number of EEG sensors decreased, but even the worst combination of prior resolution and the number of sensors was far better than the combination of no prior and the densest EEG as far as we investigated. The effect of the number of EEG sensors was small as compared to that of the resolution of the prior.

Fig. 8 shows the results of additional evaluation metrics, localization error and estimation gain, for $S_1$. For the localization error of $S_1$, two-way ANOVA revealed significant effects of the resolution of prior information [$F(2, 4499) = 1117.89$, $p<0.05$] and the number of EEG sensors [$F(2, 4499) = 62.01$, $p<0.05$] and significant interaction between these factors was not significant [$F(4, 4499) = 11.23$, $p<0.05$]. The localization error became larger as the resolution of the prior worsened and as the number of EEG sensors decreased (multiple comparison, $p<0.05$). But the effect of the number of EEG sensors was small as compared to that of the resolution of the prior. For the estimation gain of $S_1$, two-way ANOVA showed significant effects of the resolution of prior information [$F(2, 4499) = 312.95$, $p<0.05$] and the number of EEG sensors [$F(2, 4499) = 46.77$, $p<0.05$], but interaction between these factors was not significant [$F(4, 4499) = 2.35$, $p = 0.0522$]. The estimation gain decreased as the resolution of the prior worsened and as the number of EEG sensors decreased (multiple comparison, $p<0.05$). Again, the effect of the number of EEG sensors was small as compared to that of the resolution of the prior. Because both $S_1$ and $S_2$ had correct active prior information, $S_2$ showed similar results (see Tables 1 and 2). From Table 1, it can be seen that the localization error was less than the spatial resolution of the prior if the correct prior is available. From Table 2, it can be seen that the estimation gain was 0.12 even when the source current was estimated with 64-ch EEG using the correct prior with the highest resolution (R = 6).

The results of the second step can be summarized as follows. Estimation accuracy decreased as both the resolution of prior information and the number of EEG sensors, but the resolution had a larger effect than the number of sensors. However, estimation with the combination of the lowest density EEG (i.e., 19-ch) and prior resolution (i.e., R = 18) performed far better than estimation using the densest EEG (i.e., 64-ch) without prior.

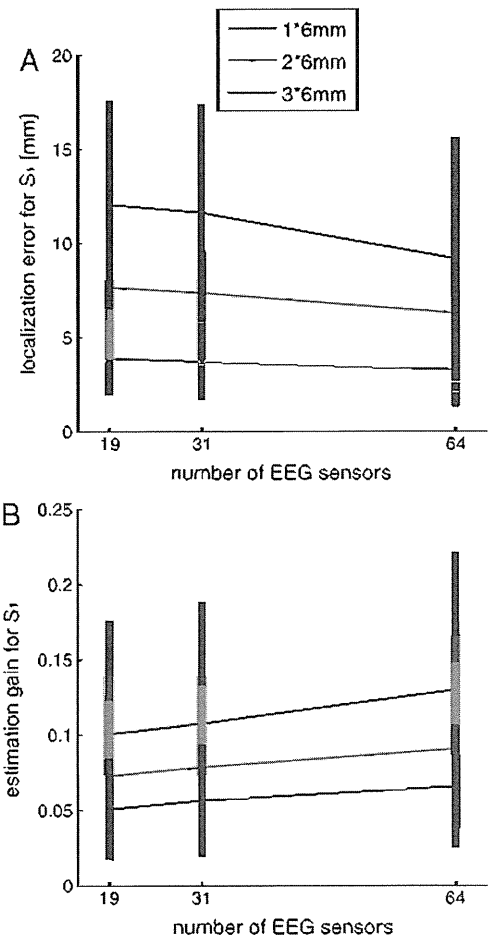


Fig. 8. Results of the second step of the simulation. (A) The localization errors for $S_1$ are plotted against the number of EEG sensors. (B) The estimation gains for $S_1$ are plotted against the number of EEG sensors. The line colors are the same as those in Fig. 6. Error bars indicate SDs.

### *Results of human scanning experiments*

#### *EEG, fMRI and NIRS activity*

Experimental data for subject RO are presented in Fig. 9. Fig. 9A shows the SMA, the PMA, the M1, and the primary somatosensory area (S1) determined using the Automated Anatomical Labeling (AAL) in the WFU PickAtlas (Maldjian et al., 2003) from structural MRI. These areas were selected as the regions of interest (ROI) for later analysis, because they are related to movement preparation/execution and somatosensory information processing.

Table 1
Localization error.

| Number of EEG sensors | 19 | 31 | 64 |
|---|---|---|---|
| $S_1$ | | | |
| R = 6 | 3.89 (1.90) | 3.72 (2.00) | 3.28 (1.95) |
| R = 12 | 7.77 (3.77) | 7.37 (3.81) | 6.29 (4.20) |
| R = 18 | 12.06 (5.52) | 11.64 (5.74) | 9.17 (6.42) |
| $S_2$ | | | |
| R = 6 | 4.02 (1.88) | 3.95 (2.21) | 3.44 (2.09) |
| R = 12 | 7.59 (3.78) | 7.54 (3.99) | 6.44 (4.06) |
| R = 18 | 12.36 (5.67) | 12.10 (5.79) | 9.64 (6.28) |

Mean localization errors from 500 combinations of sources ($S_1$ and $S_2$) are listed in millimeters. SDs are listed in parentheses.

Table 2
Estimation gain.

| Number of EEG sensors | 19 | 31 | 64 |
|---|---|---|---|
| $S_1$ | | | |
| R = 6 | 0.10 (0.08) | 0.11 (0.08) | 0.13 (0.09) |
| R = 12 | 0.07 (0.05) | 0.08 (0.05) | 0.09 (0.06) |
| R = 18 | 0.05 (0.03) | 0.06 (0.04) | 0.07 (0.04) |
| $S_2$ | | | |
| R = 6 | 0.09 (0.07) | 0.10 (0.07) | 0.12 (0.09) |
| R = 12 | 0.07 (0.05) | 0.07 (0.05) | 0.09 (0.06) |
| R = 18 | 0.05 (0.03) | 0.05 (0.03) | 0.07 (0.04) |

Mean estimation gains from 500 combinations of sources ($S_1$ and $S_2$) are listed. SDs are listed in parentheses

Fig. 9B shows the ERPs recorded at C3 and C4 of the International 10–20 system. MRPs began to increase around 600 ms before movement onset and peaked at around movement onset. The observation that the early and late components of the MRPs were lateralized towards the hemisphere contralateral to the movement, combined with the finding that the movement onset detected by the optical sensor was delayed by about 130 ms relative to that detected by EMG, suggests that the early and late components of the observed MRPs represented NS and MP, respectively. Fig. 9C shows the fMRI activity for right index finger movements; the movements activated the contralateral SM1 area. These data were used as prior information for later current estimation with VBMEG. Fig. 9D shows NIRS activity mapped to the cortical surface using Fusion software. Again, these data were also used as prior information for later current estimation. Increases in OxyHb were observed in bilateral motor-related areas. The results revealed weak lateralization towards the hemisphere contralateral to the movement. Similar results were also found for subject TA.

*Cortical current estimated by VBMEG*

The spatial pattern of the estimated cortical current was visualized by averaging the estimated current density of each dipole over the 200 ms before movement onset to focus on the brain activities involved with movement execution. The temporal pattern of the estimated current was visualized by averaging the estimated current density within each area of SMA, PMA, M1 and S1.

Fig. 10 shows results of VBMEG applied to 64-ch EEG data with fMRI prior (left), NIRS prior (middle), and no prior (right) for subject RO. Figs. 10 A and B show the spatial and temporal patterns, respectively.

Regarding the results of the fMRI prior case, the spatial pattern (Fig. 10A, left) was similar to the fMRI activity (Fig. 9C), confirming the validity of the estimation. The temporal pattern (Fig. 10 B, left) shows that current densities in the left (i.e., contralateral) PMA, M1 and S1 began to increase around 500 ms before movement onset and peaked just before movement onset. These results were consistent with the findings of previous studies that used other source localization methods with MEG data (Cheyne et al., 2006). The amplitudes of the estimated currents were higher in left M1 and S1 than in SMA and PMA, consistent with the previous studies investigating the source current from MEG during voluntary movements (Cheyne et al., 2006; Huang et al., 2004; Toda et al., 2011). In addition, the order of the estimated amplitude was comparable to that in previous studies on MEG source current in sensorimotor (Cheyne et al., 2006; Huang et al., 2004; Toda et al., 2011) and visual (Yoshioka et al., 2008) regions. Thus, the results of VBMEG applied to 64-ch EEG

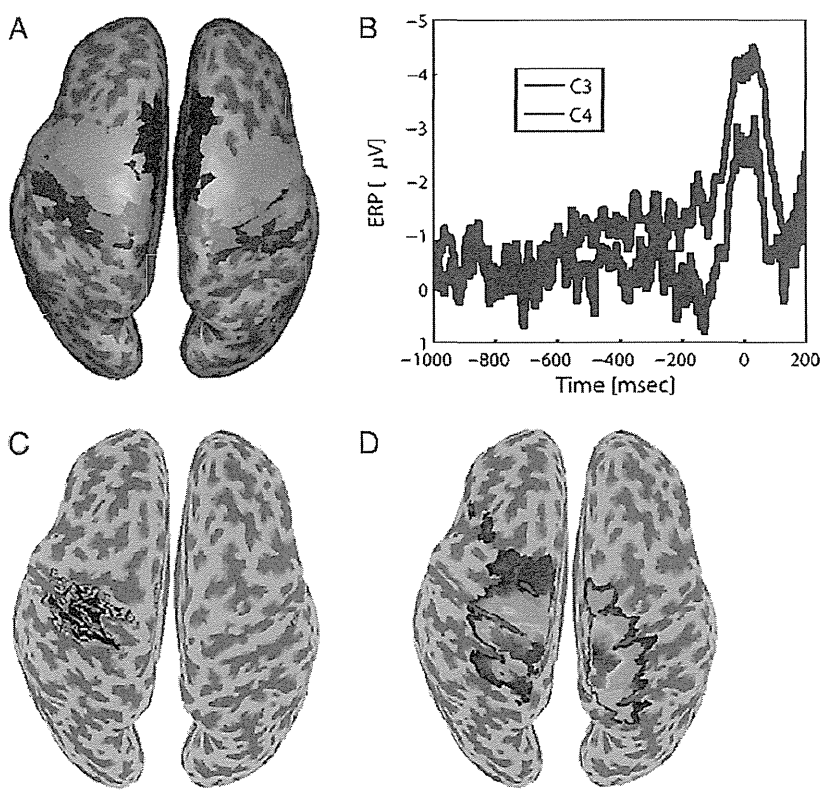


Fig. 9. Experimental data for subject RO. (A) The supplementary motor, premotor, primary motor, and primary somatosensory areas are represented by blue, yellow, green and red, respectively. (B) Event-related potentials (ERPs) for right index finger movements at C3 and C4 of the International 10-20 system. (C) fMRI activity used for prior information. (D) NIRS activity used for prior information. Note that we mapped the NIRS measurements onto the cortical surface without solving the inverse problem.

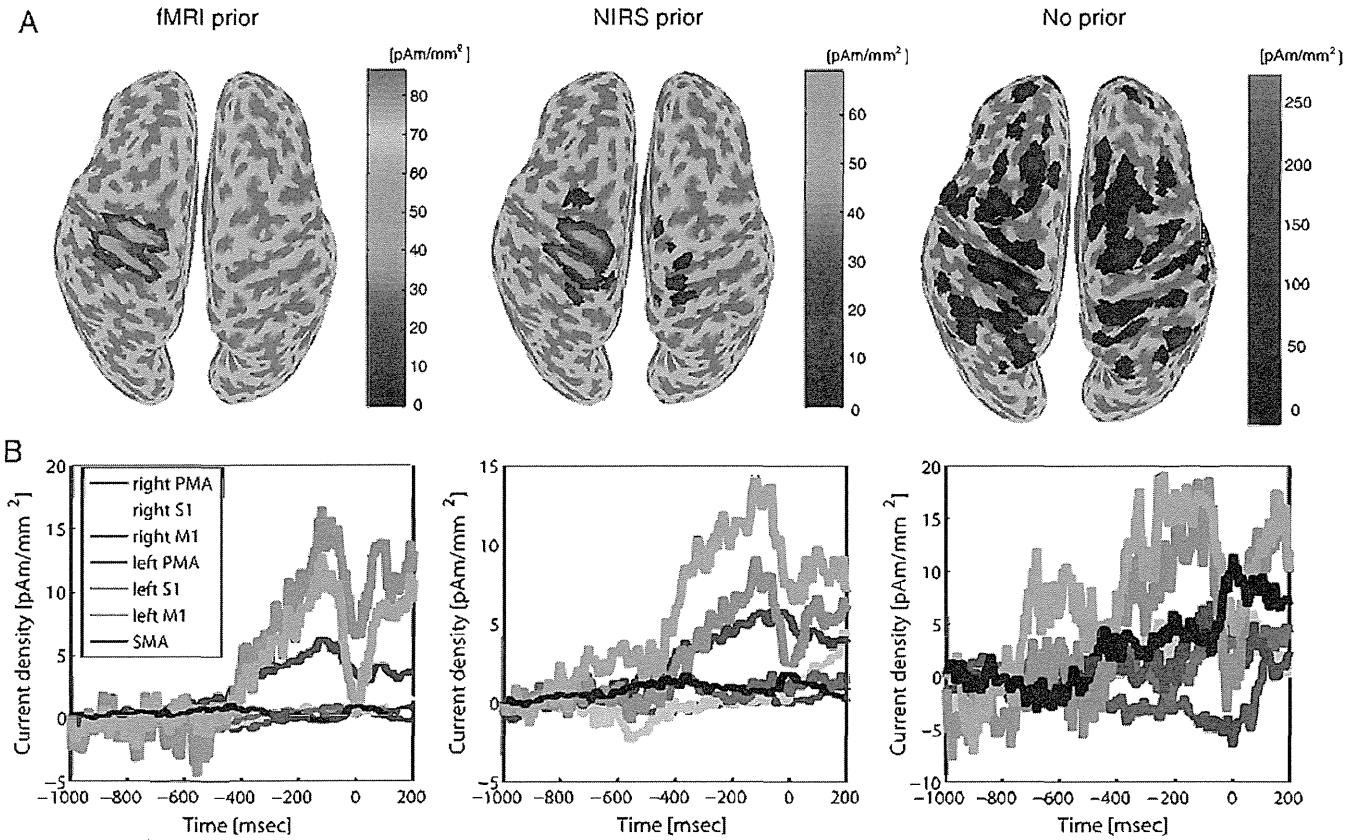


Fig. 10. Results of VBMEG under different priors. Estimations with fMRI prior, NIRS prior, and no prior are shown from left to right. (A) Spatial patterns for estimated currents averaged over a 200 ms duration just before movement onset. (B) Temporal patterns for estimated currents averaged within each area. PMA; premotor area, S1; primary somatosensory area, M1; primary motor area, SMA; supplementary motor area.

with fMRI prior were physiologically reasonable, supporting its use as a reference.

Regarding the NIRS prior case, the spatial pattern (Fig. 10A, middle) was similar to both the fMRI activity (Fig. 9C) and the spatial pattern for the case with fMRI-prior information (Fig. 10A, left), suggesting the validity of estimation with VBMEG. The temporal pattern (Fig. 10B, middle) was similar to that for cases using fMRI information as a prior, in accord with several previous reports (Cheyne et al., 2006; Huang et al., 2004; Toda et al., 2011). In addition, the order of the estimated amplitude was comparable to that in previous studies (Cheyne et al., 2006; Huang et al., 2004; Toda et al., 2011; Yoshioka et al., 2008). Thus, VBMEG applied to 64-ch EEG with NIRS prior performed relatively well.

Regarding the results of the no prior case, the spatial pattern (Fig. 10 A, right) showed that estimated current sources were located in widespread areas in addition to the activated areas indicated in the fMRI experiment (mainly left SM1, see Fig. 9C) and no clear laterality was observed. Furthermore, the temporal pattern (Fig. 10B, right) for each area was noisy, though the activities of the left M1 and S1 increased during the 500-ms period before movement onset. Thus, the performance of VBMEG with no prior information was rather poor, in accord with previous MEG study (Yoshioka et al., 2008) and the present simulation experiment.

The quantitative evaluation of the experimental data is as follows. First, we describe the effect of the types of prior information (see Fig. 10 for the qualitative evaluation). Table 3 shows that the current density pattern with the NIRS prior resembled the reference pattern (i.e., the pattern for the combination of 64-ch EEG and fMRI prior) more than the pattern with the prior in terms of spatio-temporal ($R_{st}$) and spatial correlations ($R_s$) and root mean squared errors (RMSE). This was true regardless of the number of EEG sensors. In addition, estimation using the fMRI prior performed better than that using the NIRS prior, for both 19-ch and 31-ch EEG, in terms of all of these metrics using the reference pattern. These findings are consistent with the results of the second step simulation study, indicating that estimation accuracy was increased by the use of prior information (even when the spatial resolution of prior information was low and/or when the prior included incorrect information), compared with the estimation accuracy with no prior information, and that

Table 3
Comparison of the current density pattern for each combination with the reference pattern.

| Evaluation metrics | $R_{st}$ | $R_s$ | RMSE [pAm/mm²] |
|---|---|---|---|
| fMRI prior | | | |
| 31-ch EEG | 0.76 (0.23) | 0.80 (0.23) | 5.82 (6.07) |
| 19-ch EEG | 0.44 (0.17) | 0.53 (0.09) | 12.0 (4.21) |
| NIRS prior | | | |
| 64-ch EEG | 0.40 (0.14) | 0.45 (0.13) | 5.34 (2.32) |
| 31-ch EEG | 0.18 (0.07) | 0.37 (0.15) | 9.49 (4.81) |
| 19-ch EEG | 0.18 (0.06) | 0.36 (0.12) | 9.13 (4.99) |
| No prior | | | |
| 64-ch EEG | 0.07 (0.03) | 0.08 (0.04) | 103.08 (83.18) |
| 31-ch EEG | 0.02 (0.00) | 0.03 (0.01) | 165.98 (157.57) |
| 19-ch EEG | 0.02 (0.00) | 0.02 (0.01) | 148.88 (181.26) |

Evaluation metrics which reflect similarities between the current density pattern for each combination and that for the reference (i.e., the combination of 64-ch EEG and fMRI prior) are compared. The evaluation metrics were averaged over two subjects. SDs are listed in parentheses.

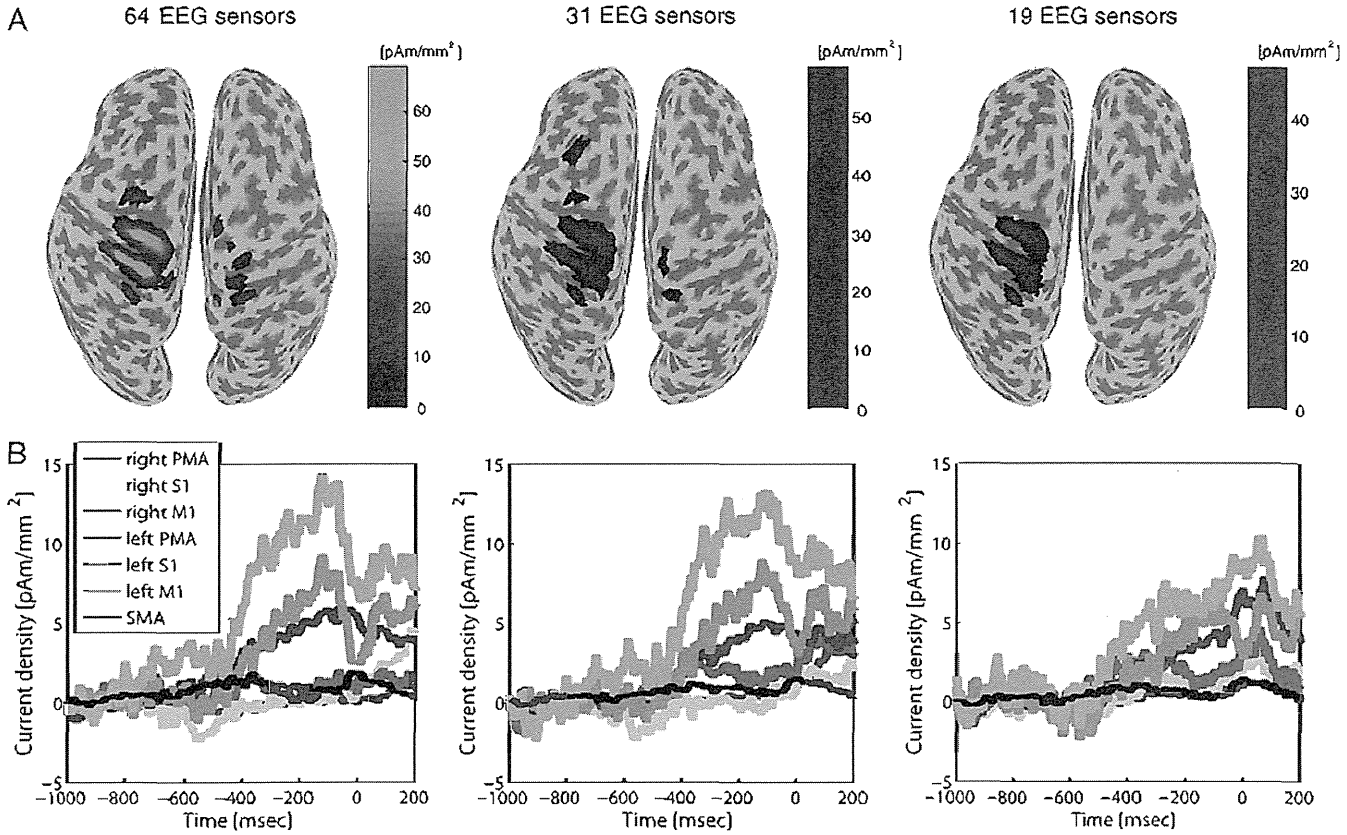


Fig. 11. Results of VBMEG with NIRS prior under different numbers of EEG sensors. Numbers of EEG sensors of 64, 31 and 19 (in reality, 62, 29 and 17 sensors, because of the rejection of extraordinary sensors) are shown from left to right. (A) Spatial patterns for estimated currents averaged over the 200 ms period just before movement onset. (B) Temporal patterns for estimated currents averaged within each area. PMA; premotor area, S1; primary somatosensory area, M1; primary motor area, SMA; supplementary motor area.

the estimation accuracy increased with the spatial resolution of prior information.

Next, we describe the effect of the number of EEG sensors (Table 3; see Fig. 11 for the qualitative evaluation) in combination with the interaction of the types of prior information and the number of EEG sensors. When the fMRI/NIRS prior was used, all evaluation metrics worsened as the number of EEG sensors decreased. These findings are consistent with the second step simulation results that estimation accuracy decreased with the number of EEG sensors when the prior is available. In addition, the combination of 19-ch EEG with the NIRS prior performed higher than that of 64-ch EEG with no prior, consistent with the simulation result that the prior information improves estimation performance even if the spatial resolution is relatively low and the number of EEG sensors is few.

## Discussion

The current study evaluated the performance of VBMEG for estimating cortical currents from EEG data, and investigated the effects of prior information and the number of EEG sensors using both computer simulations and real experiments. A summary of the results is presented below.

The data from the first step simulation suggested the following: first, as long as the magnification parameter $m_0$ was not far from the theoretical value, the estimation performance was very high when correct prior information with high spatial resolution was used. It should be noted that the SNR used in the simulations was similar to that observed in the present experiment. Second, two incorrect priors showed different effects on estimation accuracy; the false positive prior had little harmful effect, but the missing prior worsened the detection of the source, especially that with false inactive prior information. Third, estimation performance was relatively high for the most types of prior information when the moderate value of the magnification parameter ($m_0 = 100$) was used.

In the second step of the simulations, we observed that the performance of VBMEG increased with both the spatial resolution of prior information and the number of EEG sensors, but the effect of the resolution was larger. In addition, estimation accuracy was better for the combination of the lowest density (i.e., 19-ch) EEG and prior with the lowest spatial resolution (i.e., $R = 18$) than for the combination of the highest density (i.e., 64-ch) EEG and no prior.

Experimental data confirmed the following. First, both the spatial and temporal patterns of the estimated current produced physiologically plausible results if fMRI information was incorporated as a hierarchical prior. This result is consistent with the simulation findings revealing that VBMEG applied to EEG data with prior information of high spatial resolution correctly estimated the cortical current patterns, even when the noise level was similar to that in real situations. Second, the estimated current with NIRS prior information resembled that with fMRI prior information more than it resembled the estimation with no prior. This finding is also consistent with the simulation results indicating that the estimation accuracy was increased by the use of prior information (even when prior information is not very accurate), compared with the estimation accuracy with no prior information. Third, decreasing the number of EEG sensors worsened the accuracy in the fMRI/NIRS case, consistent with the second step simulation result that decreasing the number of EEG sensors slightly worsened the estimation when the prior was available. Fourth, the

current pattern for 19-ch EEG with NIRS prior was more similar to that for 64-ch EEG with fMRI prior than it was to that for 64-ch EEG with no prior information. This finding is also consistent with the simulation results.

The most important result of the present study is the demonstration that, by combining EEG and NIRS data under the framework of hierarchical Bayesian estimation, it is possible to obtain relatively high spatio-temporal, physiologically plausible, brain activity, which cannot be obtained using the individual data. Because both EEG and NIRS are associated with the merits of high portability and low sensitivity to body motion artifacts, VBMEG with combined EEG–NIRS potentially represents a powerful tool for neuroscience research. This combined method is suitable for measuring brain activity in infants or patients, for investigating brain activity related to human motor control in realistic situations (e.g., in sitting or standing positions), and for daily use, e.g., monitoring day-to-day changes in brain activity during stroke recovery or motor learning. In addition to the benefits of combining EEG and NIRS data using VBMEG, it is important to consider the potential weaknesses of VBMEG. As seen in the first step of the simulation, (1) estimation accuracy deteriorates if the wrong combination of hyper-parameters is chosen, and (2) the source with false inactive prior information was hard to be detected. These methodological weaknesses should be taken into account when interpreting the results of estimation with VBMEG.

In this study, task protocols used in EEG, NIRS and fMRI experiments were not consistent; in EEG experiments the subjects were instructed to perform a repetitive right finger movement slowly (less than 0.3 Hz), whereas in NIRS and fMRI experiments they were instructed to perform the motor task rapidly. According to previous studies, the SM1 and SMA are activated during slow-rate movements, reflecting not only the execution and somatosensory information-processing stages, but also the preparation stage, whereas SM1 is predominantly activated during fast-rate movements, mainly reflecting the late preparation, execution and somatosensory information-processing stages (Kunieda et al., 2000; Toma et al., 1999). In fact, results of our fMRI/NIRS experiments supported this. Considering our simulation result that VBMEG with missing prior exhibited difficulty in detecting the source with false inactive prior, it may problematic to use fMRI/NIRS activity directly as prior because it lacks the SMA activity. For this reason, as described in EEG experiments and preprocessing, we eliminated the EEG component reflecting the preparation stage, the BP component, using a high-pass filter of 0.2 Hz. By this preprocessing, we can focus on the brain activity common for both fMRI/NIRS and EEG experiments, SM1 activity. We therefore consider that the fMRI/NIRS prior used in the present study is almost adequate. However, using the same task in the experiments for both prior information and EEG/MEG appears to be desirable. Moreover it will be better to adopt simultaneous measurement, because when EEG and fMRI/NIRS data are obtained in different experiments, the possibility that the brain activity measured in the fMRI/NIRS experiment may not correspond precisely to that in the EEG experiment may arise even if the task in both experiments is the same. Simultaneous measurement enhances the reliability of prior information, which may improve estimation accuracy. Another merit of simultaneous measurement is that it is suitable for monitoring short-term changes in brain activity, for example, during motor adaptation. Because such changes may have little reproducibility, it is impossible to monitor them by measuring EEG/MEG and NIRS/fMRI separately. It should be noted that simultaneous measurement is technically difficult for the combination of MEG–fMRI, but is possible for EEG–NIRS. Shimadzu Corporation has already developed a simultaneous measurement system for EEG–NIRS. The present study will therefore lay the foundations for future studies using simultaneous EEG and NIRS measurement.

When the mismatch between brain activity measured by NIRS and that by EEG is caused by the task difference, simultaneous measurement will be the ideal solution. However, since the physiological sources of both modalities are different (i.e., EEG records the electrical activity and NIRS detects the hemodynamic changes), spatial characteristics of NIRS responses to evoked neural activity may not be consistent with those of EEG responses. Simulation results suggest that the reliability of estimation with VBMEG depends on the type of such physiologically mismatch; only when the active areas in EEG responses are subsets of those in NIRS responses, the estimation is reliable.

In the simulation study, the estimation accuracy of VBMEG decreased with the number of EEG sensors, though the effect of the number of EEG sensors was small as compared to that of the spatial resolution of prior. In the real experiments, the number of EEG sensors also affected the estimation accuracy when the fMRI/NIRS prior was available. This is not desirable, because it is better to reduce the number of EEG sensors to shorten the experimental time, especially in infants or patients, thus reducing the burden on the subject. However, both simulation and experimental data suggest that the combination of low-density (i.e., 19-ch) EEG and low-resolution (i.e., NIRS) prior yielded better estimation accuracy than high-density (i.e., 64-ch) EEG alone. We therefore propose that both EEG and NIRS data should be measured, at the cost of the number of EEG sensors.

In the present study, the estimated current amplitude in the experimental studies was in the order of $10^0$–$10^2$ [pAm/mm$^2$], similar to that obtained in previous studies investigating MEG source currents in sensorimotor (Huang et al., 2004; Toda et al., 2011) and visual (Yoshioka et al., 2008) regions, as well as in theoretical studies (Hamalainen et al., 1993). However, this does not indicate that the estimated amplitude is true, because the range is wide and, more importantly, the amplitude in simulation data was underestimated by approximately 10%. Theoretically, the estimation gain decreases as the estimated noise level increases. In addition, the estimation gain should be underestimated if $m_0$ used in the estimation is smaller than the theoretical value. The underestimation in the simulation study was within the range that can be explained by the effect of the noise level and the value of $m_0$ used in the estimation (note that we used $m_0 = 100$ though the theoretical value was 674). Because we set the noise level in the simulation study to be similar to that in real EEG data, the estimated amplitude in the real data may be underestimated.

As described above, the simulation results suggest that the spatial resolution of the prior information affects the accuracy of VBMEG. It is therefore important to improve the spatial resolution of NIRS measurement. To this end, the skin blood flow artifact in this study was removed by using short-distance source-detector channels, which improved the accuracy of VBMEG; estimation accuracy were low [$R_{st} = 0.256$ (0.219), $R_s = 0.288$ (0.273), RMSE = 16.2 (16.6) pAm/mm$^2$] without removing the artifacts. However, even if the skin blood artifact is completely rejected, spatial resolution and localization accuracy are limited by measurement geometry to approximately 3 cm, comparable with the distance between emitters and detectors, in the plane parallel to the scalp. The resolution limitation can be overcome only by performing diffuse optical tomography (DOT), which uses a model of photon migration through the head to obtain the activated source (Boas and Dale, 2005). The use of the NIRS prior obtained with this technique will be a matter for future research.

In the present study, we used cortical and head models constructed from structural MRI, for the following reasons. The lead field of EEG is affected by the conductivity of the skull and scalp much more than that of MEG. Therefore, interpreting EEG signals requires more precise knowledge of the thickness and conductivity of the tissues in the head. In the spherical model, concentric inhomogeneities do not affect the magnetic field at all, whereas they have to be taken into account in the analysis of EEG data (Hamalainen et al., 1993). In addition, as described in a previous study (Sato et al., 2004), the introduction of structural MRI information significantly

increased the spatial resolution of VBMEG in MEG analysis. Taken together, these findings indicate that structural MRI should be included as prior information, particularly in EEG analysis. Fortunately, once MRI data is obtained, it can be used repeatedly. In cases where MRI is unavailable, computed tomography (CT) images may provide a suitable alternative. Henson et al. (2009) compared the effect of head-models on estimation accuracy, within the context of two types of spatial prior on the sources: a single prior corresponding to a standard L2-minimum-norm (MNM) inversion, or multiple sparse priors (MSP). The study reported (1) no evidence that a cortical model derived from an individual's MRI was superior to a cortical model inverse-normalized from the Montreal Neurological Institute (MNI) template, but (2) clear evidence that a Boundary Element Model (BEM) head-model was superior to spherical head-models, provided individually-defined inner skull and scalp models were used. Because skull and scalp models can be derived from an individual's CT image, sufficient estimation accuracy may be achieved by using a combination of individual's CT images and template MRI.

In the analysis of experimental data, we used different statistics to impose spatial priors, when derived from either fMRI or NIRS; the $t$-statistic was used in the case of fMRI prior, but peak amplitude was used in the case of NIRS prior. We did not use $t$-values in the NIRS case for two reasons. First, $t$-statistics are not commonly used in the field of NIRS but they are commonly used in fMRI studies. Second, estimation with 64-ch EEG was better for the NIRS prior based on the peak values [averages (SDs) for evaluation metrics are as follows; $R_{sl}=0.40$ (0.14), $R_s=0.45$ (0.13), RMSE = 5.34 (2.32)] than for the NIRS prior based on the $t$-value [$R_{sl}=0.36$ (0.11), $R_s=0.42$ (0.09), RMSE = 5.79 (2.67)].

VBMEG with fMRI or NIRS priors revealed that current density in M1 started increasing around 500 ms before movement onset, peaking just before movement onset, and exhibiting lateralization towards the hemisphere contralateral to the movement. These results are consistent with the knowledge that the NS and MP components of MRPs arise from the contralateral M1 and are related to late preparation and execution of movements. The estimation with VBMEG from EEG with NIRS prior is therefore a useful tool for investigating motor-related cortical activity in both normal individuals and stroke patients. Activation of the SMA was weak in the present study. This may have been because we eliminated the BP component, arising predominantly from the SMA, using a high-pass filter, and/or because both fMRI and NIRS information as hierarchical priors of VBMEG exhibited little SMA activity. Future studies using simultaneous measurements of EEG and NIRS should make it possible to focus on SMA activity related to the early preparation stage, by using slow-rate movement tasks with an event-related design.

## Acknowledgments

We thank Dr. Satoshi Tanaka for helping us to carry out fMRI experiments. We also thank Dr. Ken-ichi Morishige at Toyama Prefectural University and Dr. Taku Yoshioka at ATR Neural Information Analysis Laboratories for helpful comments. This research was supported by the Strategic Research Program for Brain Sciences (SRPBS), and partially supported by the National Institute of Information and Communications Technology (NICT) and Funding Program for Next Generation World-Leading Researchers.

## Appendix A. Variational Bayesian Multimodal EncephaloGraphy (VBMEG)

### *EEG forward model*

VBMEG (Sato et al., 2004; Yoshioka et al., 2008) is one of the distributed source methods, in which the cortical current is modeled by a number of current dipoles with fixed position and orientation. The cortical dipole current directions were assumed to be perpendicular to the cortical surface. Because EEG data contains not only brain activity but also the effects of artifacts, we also placed dipoles on artifactual sources, eyes, according to previous studies (Fujiwara et al., 2009; Morishige et al., 2009). The artifact current dipoles were located in the center of the right and left eyeballs.

According to the previous study (Fujiwara et al., 2009), the EEG forward model, that is, the relationship between the amplitude of current dipoles and observed electric potential at time point $t$, is given by

$$\mathbf{E}(t) = \mathbf{G}_{\mathbf{brain}} \cdot \mathbf{J}_{\mathbf{brain}}(t) + \mathbf{G}_{\mathbf{eye}} \cdot \mathbf{J}_{\mathbf{eye}}(t) + \varepsilon(t), \tag{1}$$

where $E(t)$ is an $N\times 1$ vector for the observed electric potential (i.e., EEG), $J_{brain}(t)$ is an $L\times 1$ vector for the cortical current, and $J_{eye}(t)$ is an $K\times 1$ vector for the eye current. Constants $N$, $L$, and $K$ denote the number of sensors, brain current sources, and eye current sources, respectively. $G_{brain}$ is an $N\times L$ matrix, and $G_{eye}$ is an $N\times K$ matrix. $G_{brain}$ and $G_{eye}$ are called the lead field matrices, whose $n$, $l$-th and $n$, $k$-th elements describe the sensitivity of the $n$-th sensor when a unit dipole is set on the $l$-th and $k$-th locations. The lead field matrix for brain current sources $G_{brain}$ is calculated using a three-shell BEM head model (brain, skull, and scalp). The lead field matrix for eye current sources $G_{eye}$ is calculated by the Biot–Savart equation. Observation noise $\varepsilon(t)$ is assumed to obey a Gaussian distribution with zero mean. Note that, in the simulation study, we did not assume currents induced by eyes and therefore the forward model did not have the right hand second term.

### *Estimating current variance with VBMEG*

We use the hierarchical Bayesian estimation for current estimation (Sato et al., 2004). Assuming that the EEG observation noise follows Gaussian distribution with a spherical covariance, the EEG forward model (Eq. (1)) leads to the likelihood function:

$$P(E|J_{\mathrm{brain}},J_{\mathrm{eye}}) \propto \exp\left[-\frac{\beta}{2}\left\|E-G_{\mathrm{brain}}\cdot J_{\mathrm{brain}}-G_{\mathrm{eye}}\cdot J_{\mathrm{eye}}\right\|^2\right], \tag{2}$$

where $\beta$ denotes the inverse of the unknown variance of EEG observation noise. As for the prior probability distribution $P_0(J_{brain},J_{eye}|\alpha_{brain},\alpha_{eye})$, we assume a Normal prior:

$$P_0(J|\alpha_J) \propto \exp\left[-\frac{1}{2}\sum_{t=1}^{T} J'(t)\cdot A_J\cdot J(t)\right], \tag{3}$$

where $J'=[J_{brain}'\ J_{eye}']$, $A_J=\mathrm{diag}(\alpha_J)$, and $\alpha_J'=[\alpha_{brain}'\ \alpha_{eye}']$. Vectors $\alpha_{brain}$ and $\alpha_{eye}$ are the inverse variances of the brain and eye current sources, respectively.

The current inverse variance parameters $\alpha_J$ are estimated by introducing an Automatic Relevance Determination (ARD) hierarchical prior (Neal, 1996):

$$P_0\left(\alpha_J\right) = \prod_i \Gamma\left(\alpha_{J(i)}\middle|\overline{\alpha}_{J0(i)},\gamma_{J0(i)}\right). \tag{4}$$

where $\Gamma(\alpha|\overline{\alpha},\gamma)$ represents the Gamma distribution with mean $\overline{\alpha}$ and degree of freedom $\gamma$. $\overline{\alpha}_{J0(i)}$ is a mean prior of an inverse current variance and $\gamma_{J0(i)}$ controls the spread of the distribution of corresponding $\alpha_{J(i)}$. A prior current variance $\overline{\nu}_{J0}\equiv\overline{\alpha}_{J0}^{-1}$ represents the prior information about a current intensity. For large $\overline{\nu}_{J0}$, estimated current $\hat{J}$ could be large. For small $\overline{\nu}_{J0}$, estimated current $\hat{J}$ tends to be small. The parameter $\gamma_{J0}$ reflects the reliability (confidence) of corresponding $\overline{\alpha}_{J0}$. For very small $\gamma_{J0}$, the distribution spreads uniformly, and prior information $\overline{\nu}_{J0}$ does not affect the current estimation (non-informative prior). In contrast, for large $\gamma_{J0}$, since the distribution is concentrated around prior mean $\overline{\nu}_{J0}$, prior information $\overline{\nu}_{J0}$ influences the current estimation more strongly.

Because of the hierarchical prior, the estimation problem becomes nonlinear and cannot be solved analytically. Therefore, the approximate posterior distribution is calculated by using the Variational Bayesian (VB) method (for VB method, see Sato et al., 2004)

The $\overline{\nu}_{j0}$ and $\gamma_{j0}$ for cortical dipoles (i.e., $\overline{\nu}_{brain0}$ and $\gamma_{brain0}$) can be determined depending on whether fMRI/NIRS data are available. Here, we will explain how these were determined in the experimental data analysis.

When fMRI/NIRS data are available, the $\overline{\nu}_{brain0}$ and $\gamma_{brain0}$ were determined in the following way. We imposed fMRI/NIRS information on the prior variance parameter as: $\overline{\nu}_{brain0(l)} = \nu_0 + (m_0 - 1)\cdot\nu_0\cdot a_{(l)}^2$, where $\nu_0$ was the baseline of the prior current variance and estimated from the baseline interval of the EEG data by the minimum norm estimation (Wang et al., 1992). $a_{(l)}$ was normalized activity data ($t$-value for the fMRI case and peak value of the artifact-free Δ[OxyHb] data for the NIRS case) on the $l$-th vertex, and $m_0$ was a variance magnification parameter and set to 100 for all dipoles. We set the confidence parameter $\gamma_{brain0}$ to 10 for all dipoles.

When fMRI/NIRS data are not available, we used uniform spatial prior (i.e., $\overline{\nu}_{brain0} = m_0\nu_0$ for all cortical dipoles) where the magnification parameter $m_0$ was set to 100, and the confidence parameter $\gamma_{brain0}$ was set to 10 for all dipoles (i.e., non-informative prior).

The $\overline{\nu}_{j0}$ and $\gamma_{j0}$ for eye dipoles (i.e., $\overline{\nu}_{eye0}$ and $\gamma_{eye0}$) were set to $10^2$ [nAm]$^2$ and $10^{4.5}$, respectively, according to a previous study (Morishige et al., 2009).

*Spatial smoothness constraint*

We also assumed a spatial smoothness constraint on the current distribution along with the cortical surface (Shibata et al., 2008). For this purpose, we used a smoothing filter matrix $W_{ij} \propto \exp(-d_{ij}^2/R^2)$, where $d_{ij}$ is the distance between $i$-th and $j$-th current dipoles. The smoothing radius parameter, $R$, was set to 6 mm. By introducing an auxiliary variable $Z(t)$ and letting

$$J_{\mathrm{brain}}(t) = WZ_{\mathrm{brain}}(t), \tag{5}$$

Eq. (1) can be replaced by

$$E(t) = \tilde{G}_{\mathrm{brain}}\cdot Z_{\mathrm{brain}}(t) + G_{\mathrm{eye}}\cdot J_{\mathrm{eye}}(t) + \varepsilon(t) \tag{6}$$

where $\tilde{G} \equiv GW$ is a smoothed lead field matrix. Therefore, the EEG inverse problem is changed to estimate $Z(t)$ instead of $J(t)$, with the smoothed lead field matrix $\tilde{G}$. After estimating $Z(t)$, the actual current amplitude $J(t)$ was calculated using Eq. (5).

## Appendix B. Unbiased estimation of the AUC

For each threshold $\beta$, the number of estimated or simulated inactive dipoles was much greater than the number of active dipoles. To interpret the AUC as a detection accuracy index, the same number of active and inactive dipoles should be provided in the ROC analysis (Grova et al., 2006).

Let $\Theta$ define the set of all cortical dipoles ($\mathrm{card}(\Theta) = p$) and $\Theta_a$ define the set of simulated active dipoles ($\mathrm{card}(\Theta_a) = p_a$). To provide less biased estimation of ROC parameters, we randomly chose a set $\Theta_f$ of $p_a$ fictive dipoles among the $p - p_a$ remaining inactive dipoles, i.e., $\Theta_f \in \Theta \backslash \Theta_a$. Less biased ROC curves and AUC were then estimated for those sets of $p_a$ pairs of active $\Theta_a$ and fictive $\Theta_f$ dipoles.

However, the false positive rate may now be greatly underestimated because many spurious active dipoles are missed by the random drawing of $\Theta_f$ in $\Theta \backslash \Theta_a$. We thus adopted two strategies to choose $\Theta_f$, optimizing the false positive detection. We split the estimation of detection accuracy into two components, one dedicated to the localization ability of the method and the second dedicated to false positive detection far from the simulated active dipoles.

For the localization ability, a criterion $\mathrm{AUC}_{\mathrm{close}}$ was estimated by choosing the fictive dipoles within a 5-cm radius sphere[5] centered on the simulated active dipole, i.e., $\Theta_f \in \Theta^{sphere}(\Theta_a) \backslash \Theta_a$, where $\Theta^{sphere}(\Theta_a)$ denotes the set of dipoles within a 5-cm radius sphere centered on the simulated active dipole. For the detection of false positive far from the simulated source, a criterion $\mathrm{AUC}_{\mathrm{far}}$ was estimated by choosing the fictive dipoles among dipoles far from the simulated active source, i.e., within the complementary set of $\Theta^{sphere}(\Theta_a)$: $\Theta_f \in \Theta \backslash \Theta^{sphere}(\Theta_a)$.

The proposed index of detection accuracy AUC was then defined as the mean of the previous criteria:

$$\mathrm{AUC} = \frac{1}{2}(\mathrm{AUC}_{\mathrm{close}} + \mathrm{AUC}_{\mathrm{far}}).$$

To obtain consistent measurements not sensitive to one particular choice of $\Theta_f$, AUC was estimated over 100 independent drawings of $\Theta_f$. The mean AUC over those 100 trials will be presented here as an index of detection accuracy.

## Appendix C. How to determine the cortical projection point of each NIRS channel

When the NIRS channel is on a gyrus, the cortical vertex that is the closest from the channel should be found as a single point (see Fig. 2F of Okamoto et al., 2004). In this case, we defined the vertex as a cortical projection point of the channel. When the NIRS channel is on a sulcus, we selected two to four cortical vertices on the gyri that sandwich or surround the sulcus and represent local minimum distances (see Figs. 2G–I of Okamoto et al., 2004). To the line defined by the two minimum-distance vertices or to the plane defined by the three minimum-distance vertices, we drew a normal line from the channel. We defined a cortical projection point as the point at which the normal line intersects the cortical surface (see Figs. 2F–I of Okamoto et al., 2004). In some extreme cases where we found four minimum-distance vertices, we drew two lines defined by two neighboring, non-overlapping vertices. We next drew normal lines from the channel to the two lines and obtained two separate intersections. By reducing four vertices to two, we could apply the procedure above. Similarly, we tested the other combination of two lines, and applied the average value of the two combinations.

## Appendix D. Interpolation method of the NIRS data

The inverse distance weighting (IDW) method (Shepard, 1968) was used to interpolate a NIRS value ($a_{(l)}$) at the $l$-th cortical vertex (interpolation point) on the brain using known normalized NIRS values at scattered known neighborhood cortical projection points (Takeuchi et al., 2009). The value $a_{(l)}$ is obtained based on a following interpolating function:

$$a_{(l)} = \frac{\sum_{i=1}^{n} w_i f_i}{\sum_{i=1}^{n} w_i}$$

where $n$ is the number of the neighborhood cortical projection points, $w_i$ is a weight function assigned to each neighborhood cortical projection point, and $f_i$ is a known normalized NIRS value at a known cortical projection point of the corresponding NIRS channel.

[5] Grova et al. (2006) did not adopt the 5-cm radius sphere centered on the source, but adopted the 10-th neighborhood of the source to calculate $\mathrm{AUC}_{\mathrm{close}}$ and $\mathrm{AUC}_{\mathrm{far}}$. However, the region including the 10-th neighborhood will be different between our case and the case of Grova et al. (2006), because the density of cortical dipoles is different. Table 1 of Grova et al. (2006) suggests that the 5-cm radius sphere is comparable to the 10-th neighborhood. Therefore, we adopted the 5-cm radius sphere.

The weight function is obtained from the following equation:

$$w_i = \frac{1}{d_i^2}$$

where $d_i$ is distance between the known cortical projection point and the interpolation point. The number of neighborhood cortical projection points determines how many NIRS channel points with the known NIRS values are included in the IDW. This number can be specified in terms of a radius (2 cm in this paper), where a center of the circle is the given interpolation point with $a_{(i)}$. Thus, the vertices more than 2 cm away from all the projection points had no NIRS values.

## References


Boas, D.A., Dale, A.M., 2005. Simulation study of magnetic resonance imaging-guided cortically constrained diffuse optical tomography of human brain function. Appl. Opt. 44, 1957–1968.

Cheyne, D., Bakhtazad, L., Gaetz, W., 2006. Spatiotemporal mapping of cortical activity accompanying voluntary movements using an event-related beamforming approach. Hum. Brain Mapp. 27, 213–229.

Cunnington, R., Iansek, R., Bradshaw, J.L., Phillips, J.G., 1996. Movement-related potentials associated with movement preparation and motor imagery. Exp. Brain Res. 111, 429–436.

Dale, A.M., Fischl, B.R., Sereno, M.I., 1999. Cortical surface-based analysis. I: segmentation and surface reconstruction. NeuroImage 9, 179–194.

Dale, A.M., Liu, A.K., Fischl, B.R., Buckner, R.L., Belliveau, J.W., Lewine, J.D., Halgren, E., 2000. Dynamic statistical parametric mapping: combining fMRI and MEG for high-resolution imaging of cortical activity. Neuron 26, 55–67.

Daunizeau, J., Grova, C., Marrout, J., Marrelec, G., Clonda, D., Goulard, B., Pelegrini-Issac, M., Lina, J.-M., Benali, H., 2005. Assessing the relevance of fMRI-based prior in the EEG inverse problem: a Bayesian model comparison approach. IEEE Trans. Signal Process. 53, 3461–3472.

Fujiwara, Y., Yamashita, O., Kawawaki, D., Doya, K., Kawato, M., Toyama, K., Sato, M.A., 2009. A hierarchical Bayesian method to resolve an inverse problem of MEG contaminated with eye movement artifacts. NeuroImage 45, 393–409.

Grova, C., Daunizeau, J., Lina, J.-M., Benar, C.G., Benali, H., Gotman, J., 2006. Evaluation of EEG localization methods using realistic simulations of interictal spikes. NeuroImage 29, 734–753.

Grova, C., Daunizeau, J., Kobayashi, E., Bagshaw, A.P., Lina, J.-M., Dubeau, F., Gotman, J., 2008. Concordance between distributed EEG source localization and simultaneous EEG-fMRI studies of epileptic spikes. NeuroImage 39, 755–774.

Hamalainen, M., Hari, R., Ilmoniemi, R.J., Knuutila, J., Lounasmaa, O.V., 1993. Magnetoencephalography – theory, instrumentation, and applications to noninvasive studies of the working human brain. Rev. Mod. Phys. 65, 413–497.

Hari, R., 1991. On brain's magnetic responses to sensory stimuli. J. Clin. Neurophysiol. 8, 157–169.

Henson, R.N., Mattout, J., Phillips, C., Friston, K.J., 2009. Selecting forward models for MEG source-reconstruction using model-evidence. NeuroImage 46, 168–176.

Henson, R.N., Flandin, G., Friston, K.J., Mattout, J., 2010. A parametric empirical Bayesian framework for fMRI-constrained MEG/EEG source reconstruction. Hum. Brain Mapp. 31, 1512–1531.

Hoshi, Y., Kobayashi, N., Tamura, M., 2001. Interpretation of near-infrared spectroscopy signals: a study with a newly developed perfused rat brain model. J. Appl. Physiol. 90, 1657–1662.

Huang, M.X., Harrington, D.L., Paulson, K.M., Weisend, M.P., Lee, R.R., 2004. Temporal dynamics of ipsilateral and contralateral motor activity during voluntary finger movement. Hum. Brain Mapp. 23, 26–39.

Kajihara, S., Ohtani, Y., Goda, N., Tanigawa, M., Ejima, Y., Toyama, K., 2004. Wiener filter-magnetoencephalography of visual cortical activity. Brain Topogr. 17, 13–25.

Kumeda, T., Ikeda, A., Ohara, S., Yazawa, S., Nagamine, T., Taki, W., Hashimoto, N., Shibasaki, H., 2000. Different activation of presupplementary motor area, supplementary motor area proper, and primary sensorimotor area, depending on the movement repetition rate in humans. Exp. Brain Res. 135, 163–172.

Maldjian, J.A., Laurienti, P.J., Kraft, R.A., Burdette, J.H., 2003. An automated method for neuroanatomic and cytoarchitectonic atlas-based interrogation of fMRI data sets. NeuroImage 19, 1233–1239.

Michel, C.M., Murray, M.M., Lantz, G., Gonzalez, S., Spinelli, L., Grave de Peralta, R., 2004. EEG source imaging. Clin. Neurophysiol. 115, 2195–2222.

Morishige, K., Kawawaki, D., Yoshioka, T., Sato, M.A., Kawato, M., 2009. Artifact removal using simultaneous current estimation of noise and cortical sources. Lecture notes in computer science: ICONIP 2008. Springer-Verlag, Berlin, pp. 335–342.

Mosher, J.C., Lewis, P.S., Leahy, R.M., 1992. Multiple dipole modeling and localization from spatio-temporal MEG data. IEEE Trans. Biomed. Eng. 39, 541–557.

Neal, R.M., 1996. Bayesian Learning for Neural Networks. Springer-Verlag, NewYork.

Okada, E., Firbank, M., Schweiger, M., Arridge, S.R., Cope, M., Delpy, D.T., 1997. Theoretical and experimental investigation of near-infrared light propagation in a model of the adult head. Appl. Opt. 36, 21–31.

Okamoto, M., Dan, H., Sakamoto, K., Takeo, K., Shimizu, K., Kohno, S., Oda, I., Isobe, S., Suzuki, T., Kohyama, K., Dan, I., 2004. Three-dimensional probabilistic anatomical cranio-cerebral correlation via the international 10–20 system oriented for transcranial functional brain mapping. NeuroImage 21, 99–111.

Ou, W., Nummenmaa, A., Ahveninen, J., Belliveau, J.W., Hamalainen, M.S., Golland, P., 2010. Multimodal functional imaging using fMRI-informed regional EEG/MEG source estimation. NeuroImage 52, 97–108.

Phillips, C., Rugg, M.D., Friston, K.J., 2002. Anatomically informed basis functions for EEG source localization: combining functional and anatomical constraints. NeuroImage 16, 678–695.

Rosa, M.J., Daunizeau, J., Friston, K.J., 2010. EEG-fMRI integration: a critical review of biophysical modeling and data analysis approaches. J. Integr. Neurosci. 9, 453–476.

Sato, M.A., Yoshioka, T., Kajihara, S., Toyama, K., Goda, N., Doya, K., Kawato, M., 2004. Hierarchical Bayesian estimation for MEG inverse problem. NeuroImage 23, 806–826.

Schmidt, D.M., George, J.S., Wood, C.C., 1999. Bayesian inference applied to the electromagnetic inverse problem. Hum. Brain Mapp. 7, 195–212.

Shepard, D., 1968. A two-dimensional interpolation function for irregularly-spaced data. Proceedings of the 23rd National Conference ACM. ACM Press, New York, pp. 517–524.

Shibata, K., Yamagishi, N., Goda, N., Yoshioka, T., Yamashita, O., Sato, M.A., Kawato, M., 2008. The effects of feature attention on prestimulus cortical activity in the human visual system. Cereb. Cortex 18, 1664–1675.

Strangman, G., Culver, J.P., Thompson, J.H., Boas, D.A., 2002. A quantitative comparison of simultaneous BOLD fMRI and NIRS recordings during functional brain activation. NeuroImage 17, 719–731.

Takeuchi, M., Hori, E., Takamoto, K., Tran, A.H., Satoru, K., Ishikawa, A., Ono, T., Endo, S., Nishijo, H., 2009. Brain cortical mapping by simultaneous recording of functional near infrared spectroscopy and electroencephalograms from the whole brain during right median nerve stimulation. Brain Topogr. 22, 197–214.

Toda, A., Imamizu, H., Kawato, M., Sato, M.A., 2011. Reconstruction of two-dimensional movement trajectories from selected magnetoencephalography cortical currents by combined sparse Bayesian methods. NeuroImage 54, 892–905.

Toma, K., Honda, M., Hanakawa, T., Okada, T., Fukuyama, H., Ikeda, A., Nishizawa, S., Konishi, J., Shibasaki, H., 1999. Activities of the primary and supplementary motor areas increase in preparation and execution of voluntary muscle relaxation: an event-related fMRI study. J. Neurosci. 19, 3527–3534.

Waberski, T.D., Buchner, H., Lehnertz, K., Hufnagel, A., Fuchs, M., Beckmann, R., Rienacker, A., 1998. The properties of source localization of epileptiform activity using advanced head modelling and source reconstruction. Brain Topogr. 10, 283–290.

Wang, J.Z., Williamson, S.J., Kaufman, L., 1992. Magnetic source images determined by a lead-field analysis: the unique minimum-norm least-squares estimation. IEEE Trans. Biomed. Eng. 39, 665–675.

Yoshioka, T., Toyama, K., Kawato, M., Yamashita, O., Nishina, S., Yamagishi, N., Sato, M.A., 2008. Evaluation of hierarchical Bayesian method through retinotopic brain activities reconstruction from fMRI and MEG signals. NeuroImage 42, 1397–1413.

精神神経学雑誌　第113巻　第7号（毎月25日発行）　1956年4月12日　第三種郵便物認可　ISSN 0033-2658

Psychiatria et Neurologia Japonica

# 精神神経学雑誌

精神経誌　Psychiat. Neurol. Jap.

2011　VOL. 113　NO. 7



日本精神神経学会

精神神経学雑誌　第113巻第7号（2011）　662-671頁

討　　論

# 「診療選択肢評価図」を用いた精神科臨床意思決定の可視化の試み

太田　敏男[1)]，吉田　寿美子[2)]，綱島　宗介[3)]，
戸塚　貴雄[1)]，渡邉　貴文[1)]，豊嶋　良一[1)]

Toshio Ota, Sumiko Yoshida, Sousuke Tsunashima, Takao Totsuka, Takafumi Watanabe, Ryoichi Toyoshima : Visual Presentation of Psychiatric Clinical Decision-making by "Graphic Assessment Sheet for Diagnoses and Treatments"

精神科診療において，外来初診時や入院初期などの場合，病歴や検査などの情報把握が時間的に間に合わない，病気が初期段階にあるため典型的症状が出揃っていない，などの理由で，情報の不完全な状況に遭遇することは多い．しかし，それでも医師は，その時点において，得られている情報を活用して何らかの合理的判断と対処をしなければならない．こうした不完全情報下での合理的判断と対処，すなわち意思決定を行うための枠組みは，昨今のわが国の精神科診療において，ますますその重要性を増している．その理由として，新臨床研修の開始によって経験や目的意識の異なる医師の併診の機会が格段に増え，精神科医療の不完全さが残存する中で理解の食い違いが生じやすくなっていること，昨今ますます患者や家族に対する正確な説明が求められるようになっていること，などが挙げられる．筆者は，以前，不完全情報下での意思決定の枠組みとして，ベイズ統計学に基づく意思決定問題の枠組みについて述べた．今回は，上記のような背景から，この枠組みを「診療選択肢評価図」として可視化することにより不完全情報下での意思決定イメージを医師間で共有しやすくすることを試みた．具体的には，意思決定のための諸要因や変数を1枚の図に配置し，診断選択肢の確率や対処選択肢の利益・不利益の程度を視覚的に示せるように工夫した．本稿では，まず「診療選択肢評価図」について単純な仮想症例などで説明し，ついで急性期病棟の実症例における試行を提示した．最後に，本方法の有用性，限界，今後の課題などについても考察した．

<索引用語：精神科，不完全情報，臨床的意思決定，可視化，コミュニケーション>

## I．はじめに

精神医療において，個々の症例が類型化し切れない個別性を持つことは，しばしば指摘されるところである．精神現象の表現形がさまざまな文化や個人の生活背景に依存することを考慮すれば，それは当然のことであろう．しかし，そうではあっても，診断という類型化の重要性は揺らぐものではない．多くの類型化の中でも，方向性決定という面で診断が最も重要であることは，言を待たない．

ところで，精神科の急性期病棟や初診外来などで仕事をしていると，特に患者との出会い初期に

著者所属：1) 埼玉医科大学神経精神科，Department of Neuropsychiatry, Saitama Medical School
2) 独立行政法人国立精神・神経医療研究センター病院精神科，National Center Hospital of Neurology and Psychiatry
3) 医療法人社団宗仁会武蔵野病院，Sojinkai Musashino Hospital

受理日：2011年4月2日

おいて，診断に関連して重要な問題に行き当たる．それは情報の不足や不確かさという問題である[7]．その問題の由来として，第1に，病歴，症状，検査所見などの情報がまだ判明していないために量的にも質的にも限定されていることが挙げられる（「病態判明プロセス」[8]）．これはsituation variance，information variance[9]などに相当することがらとも言える．第2に，より深刻なこととして，精神疾患が初期段階にあるために症状が展開し切っていない場合のあることが挙げられる（「疾患展開プロセス」[8]）．これはsubject variance[9]に相当するとも解釈できる．例えば，統合失調症初期には，典型的な幻聴，興奮，錯乱などは存在せず，微妙な自他対立感や閉じ籠もりといった症状しか見られないことがある．うつ病でも，初期に特有な非特異的身体症状のみが先行する症例をときどき見かける．

情報の限られたこうした段階では，「基準に基づいて診断を確定し，その診断に基づいて治療する」という枠組みは，必ずしも役に立たない．なぜなら，すでに指摘したように，そもそもこの段階では情報不足で診断は確定しえないのであるが，我々医師は，確定する前であってもその時点時点において，それまでの情報を最大限に生かしたうえで，可能な限り今後を予測し，本人や家族にその段階での見通しを説明し，看護師に必要な指示を出し，処方を書き，注射や緊急検査をオーダーしなければならないからである．

筆者は，今日の未熟な段階の精神医学において，診療は多かれ少なかれ不完全情報下[5]で行われること[6]，そして「分類問題の枠組み」よりもベイズ統計学[5]の構造に準拠した「意思決定問題の枠組み」が重要であることを論じた[7]．その際，単にその時点で対症療法や状態像治療を行うだけでは不十分であり，将来展開しえる複数の疾患を具体的に想定したうえで治療を組み立てることが重要であることを強調した．また，その議論の延長として，ひとつの病態に対して複数の疾患の確率数値セット，すなわちベクトルを与え，そのベクトルを診断とみなす「ベクトル診断」の考え方を紹介した[8]．

昨今，「意思決定問題の枠組み」や「ベクトル診断」のような考え方は，重要性を増していると実感する．そのひとつの要因として，数年前に始まった新臨床研修が挙げられる．これにより，経験の豊富な専門医，経験数年程度の中間的指導医，後期研修医，1～2ヶ月だけ回る初期研修医といった極端に経験・立場に差のある医師が，不完全情報下で同じ患者を診る機会が増えている．もうひとつの要因として，人々の権利意識の高まりとともに，受療者側との意思疎通の重要性が高まったことが挙げられる．たとえ不完全情報下ではあっても，医師は受療者側に対して説明をしなければならない．しかし，この状況で実態に合わない確定的な説明をすることは，時として危険を伴う．実態が不完全情報下であるときには，それを前提とした枠組みに準拠し，実態をそのまま説明するべきであろう．

そこで，筆者は，「意思決定問題の枠組み」[7]や「ベクトル診断」[8]を診療現場に容易かつ効果的に導入する工夫を試みた．具体的には，意思決定のための要因とその関連を視覚的に1枚の図に配置する方法を考えた．そして，急性期病棟症例で若干の試行を行った．本稿では，その方法を単純な仮想症例で提示し，次いで実症例での試行を述べ，最後に有用性，限界，今後の課題などについて考察してみたい．

なお，今回作成した図示法は，表構造の一部を図式化したものなので図と表の両側面を有しているが，ここでは図示という面を重視し，「診療選択肢評価図（略して単に「評価図」）と呼ぶことにする．また，ベイズ統計学の真骨頂のひとつは，事前確率と追加情報からベイズ定理に基づいて事後確率を得る数値的プロセスであるが[1,2,5,6]，これは図示法を提示するという本稿の主題からは外れるので，割愛する．

表1 診療状況の構造と意思決定問題の構造との対比

| 診　療 | ベイズ的意思決定 |
|---|---|
| 疾患 | 自然の状態 |
| 治療 | 行動 |
| 治療結果<br>改善，治癒<br>悪化，死亡，副作用 | 価値<br>効用<br>損失 |
| 初期診断（または診断の出現頻度） | 事前確率 |
| 経過観察や検査所見 | 追加情報 |
| 観察・検査後の診断 | 事後確率 |

## II．診療選択肢配置図の構成要素，配置，およびその応用

### (1)診療状況の構造

まず，診療状況を構成する部品（要素）を意思決定過程と対比して，表1に示す（太田(2000)[7]から引用）．

初期段階における診療選択肢評価図で必要な主要構成部品は，表のうち，上から4行，すなわち疾患，治療，治療結果〔効用（改善，治癒など）と損失（悪化，死亡，副作用など）〕，および初期診断〔事前確率〕である．まず，初期情報により想定される1病態ごとに可能性のある複数の疾患が列挙される．そのそれぞれの疾患の可能性の評価が初期診断であり，確率論的表現[5]を使えば，事前確率である．治療も複数の選択肢がある．そして各治療選択肢の効用と損失がそれぞれの疾患ごとに事前に想定される．

これらの中で問題となるのは，初期診断（事前確率）のデータも治療選択肢別・診断別の効用・損失のデータもほとんどないという現実である．これは医療だけの問題ではなく，事業経営（特にベンチャー企業）のような場合でも，ベイズ統計学を応用する際に起こりえる問題である．ベイズ統計学[5]では，このような場合，個人的経験に基づく「主観的確率」[3~5]を導入する．福井[1]は，診療状況について，「“非常に高い確率で”とか，“おそらく”，“可能性あり”，などといったあいまいな言葉のかわりに，何らかの検査を行う前の事前確率は，0.9，0.75，0.5，0.25，0.1程度の大まかな数値で考えるようにすれば，定量的な事後確率の推測は十分可能となろう」と述べているが(p. 72)，これも一種の主観的確率である．もちろん，疾患の事前確率は，外来初診や入院時の疾患統計があればそれを用いることができるし，治療の効用や危険も統計を蓄積することはできる．そうしたデータが利用可能であれば，当然ながら，そちらを優先するべきである．

初期段階の事前確率は，一定期間の診察・検査後に，その間の追加情報により，ベイズ定理に基づいてより事実に近い事後確率に修正される[1,2,5,7,8]．これはそのさらにあとの診察・検査にとっては事前確率となり，さらに追加情報で修正を受けていく．

診療状況におけるこれらの部品の必要性について，症例を挙げて説明する．

【症例1】47歳の女性．某年12月入院．

1．興奮および錯乱様状態にて当科外来から入院となった．一度精神科入院歴があり，外来時診断は心因反応疑いで，きっかけは法事であった．今回も法事を契機として異常言動が出現した．泣き喚き，まとまりが悪い．本人はそうした言動を想起できないこともある．また，若い頃に「霊が見える，声が聞こえる」といったエピソードのあったことも判明している．

2．入院ごく初期の主治医団のミーティングで，指導医が「入院後によく観察した結果，興奮・錯乱は消褪しているのにまとまりがあまりに悪い．若いときに幻聴様の症状もあったし，一応統合失調症も念頭に置いた方がいい」という意見を述べた．回診医（筆者）も治療的有用性という見地から賛同した．

3．ミーティング直後の当科定例カンファランスで，担当研修医は，「心因反応ということでの入院でしたが，統合失調症の妄想型だと考えています」と説明した．

4．外来担当医は，「私は解離性障害の可能性の

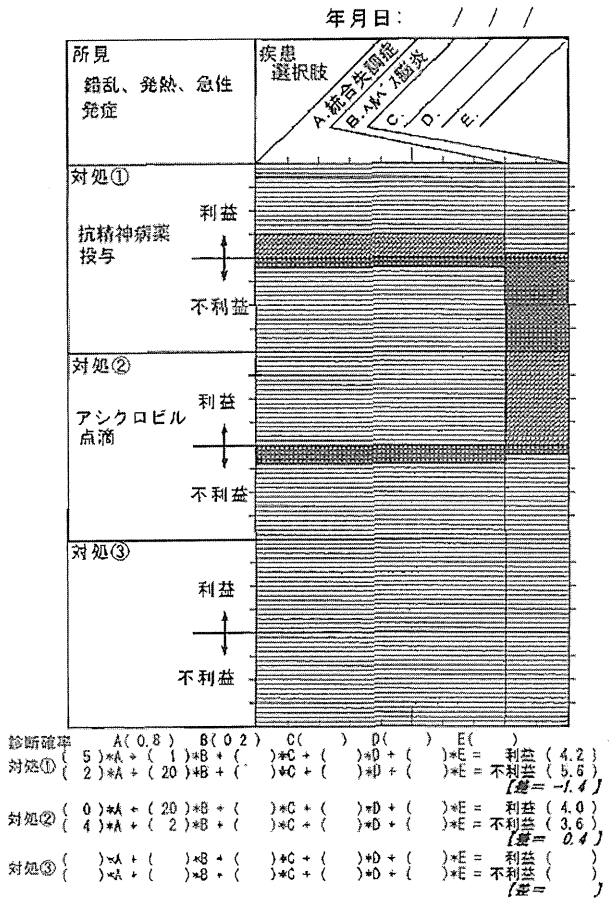


図1

方が強いと考えている．被暗示性も強い」とコメントした．

この議論を聞いて筆者は，研修医の受け取り方だけが大きく外れており，他の3者は，言葉は違うものの，考えていることは案外近いのではないか，と感じた．

具体的には，筆者は下記のように推測した．

5. 外来医はその時点までの情報で診断を，反応性の解離性障害と結論づけていた（従来病名「心因反応」の範疇）．
6. 指導医は，思路障害がかなり目立つという自身の観察結果，若い頃から幻聴様体験があったという陳述，などを追加情報とし，統合失調症をも念頭に置く必要性を感じた．ただし，それはあくまでも，統合失調症を見逃すことによる損失を大きく見積もってのことであって，統合失調症の可能性（数学的確率）自体が非常に大きいと考えたわけではなかった．統合失調症を想定したいと発言したのは，指導的意味合いを込めてのことであった．
7. 筆者（回診医）は，意思決定過程の枠組みを意識していたので[7]，その見地から指導医の方針を支持する発言をした．
8. 研修医は，指導医や回診医の，疾患の数学的確率と対処の価値とを別に考えるという考え方が理解できていなかった．その結果，指導医の「統合失調症をも考えなければならない」という文言のみが頭に残った．そして，外来医の「解離性障害」という診断を指導医が「統合失調症」に変更したと曲解した．
9. 指導医自身も，疾患の数学的確率と対処の価値との分離を明確には意識していなかった．そのため，研修医の曲解は訂正されないままになってしまった．

この例は，診断未確定の状況において精神科ベテラン医師は意識するか否かにかかわらず「意思決定問題の枠組み」[7]で考えていること，研修医はそういう考え方に慣れていないこと，そして判断の枠組みの違いにより理解のすれ違いが起こりえることを示している．このことから，診療状況における判断の枠組みを関係者に見える形で提示することの重要性がうかがえる．

### (2)診療選択肢評価図の構成：仮想症例による説明

診療選択肢評価図は，診療状況における判断の諸要素を1枚の図に配置し，判断の枠組みを視覚的に提示できるように工夫したものである．まず，この評価図の使い方を，単純な仮想症例を用いて説明する．

【仮想症例】発熱を伴う錯乱状態患者

この仮想症例は，筆者が以前[7]述べたケースをそのまま用いたもので，「救急入院となった発熱を伴う急性錯乱状態患者」である．評価図を図1に示す．作成時点は入院当日とする．

1. 疾患選択肢はA．統合失調症とB．ヘルペ

ス脳炎とする．

2．疾患の確率はそれぞれ0.8，0.2とする．

3．対処選択肢は①抗精神病薬投与と②アシクロビル点滴とする．

4．対処選択肢ごとの治療結果の見通し，すなわち利益と不利益は，以下のように想定する．説明のための例なので，ここでは数値の妥当性は議論しない．

①対処選択肢＝抗精神病薬投与

A．疾患が統合失調症だったとした場合
利　益：5（症状改善が見込めるから）
不利益：2（薬の副作用があるから）

B．疾患がヘルペス脳炎だったとした場合
利　益：1（多少の鎮静が得られる）
不利益：20（治療が手遅れになる）

②対処選択肢＝アシクロビル点滴

A．疾患が統合失調症だったとした場合
利　益：0（効果はまったくない）
不利益：4（治療遅延，経済的コスト）

B．疾患がヘルペス脳炎だったとした場合
利　益：20（脳の非可逆的侵襲の回避）
不利益：2（経済的コスト）

ここで，利益と不利益の数値に単位はなく，相対的なものである．頭に描いた判断がイメージ化できていることが重要である．

さて，我々が決断すべきは，どちらの対処選択肢を選ぶかということである．その基準となるのは，図で，斜線部分（薄く見える部分）すなわち利益の期待値が格子部分（濃く見える部分）すなわち不利益の期待値よりどれくらい大きいかである．「利益－不利益」を「実質利益」と呼ぶことにして言い換えると，実質利益の期待値が最大となる対処選択肢を選ぶことである．疾患確率は統合失調症の方が高いが，斜線部分の優位性はヘルペス脳炎の治療である対処②の方が若干上のようにみえる．計算してみると，図の説明に示すように，①抗精神病薬投与の実質利益の期待値（斜線の総面積－格子の総面積）は－1.4，②アシクロビル点滴のそれは0.4となり，やはり②の方に軍配が上がる．

(3)応用例

次に，実際例に応用してみる．複数の医師が同じ時点で横断的に評価した場合と1人の医師が縦断的に2回評価した場合とを挙げる．

3-1．横断的評価：同じ時点での複数人評価

【症例2】52歳の女性．某年11月某日入院．

入院時点までに得られた所見の要点は以下のようであった．

・30歳代から他罰的言動があったが，詳細は不明．
・近年閉じこもりがち．近所の植木の枝に対して攻撃的な電話，親戚に対して被害的な言辞などが目立つ．
・4月「電波で嫌がらせをされる」，精神科受診，糖尿病も発覚．
・10月下旬異常言動のために近所から警察通報されたことあり．
・生活行動上，「電波，指令，妖怪」といった発言が目立つ．体調不良を被害的に解釈．作為体験，幻聴的行動，攻撃的，家事はやるが洗濯が異常に執拗．
・入院時，表情や態度は硬く，ラポールが悪い．しかし，礼節は保持され，思路障害は目立たない．病識はない．
・心因は不明．

この症例について，（後期）研修医と指導医に入院時点の評価や判断について，評価図に記入を求めた．筆者自身（回診医）も記入した．図2に3者の評価図を示す．

指導医は図2aのように考えた．疾患選択肢は，A．統合失調症，B．血管性の脳器質性疾患，C．糖尿病性の症状性疾患，D．認知症，E．その他の5つで，各疾患の主観的確率は図のように0.6，0.1，0.1，0.1，0.1であった．また，対処選択肢として，①経過観察，②抗精神病薬，そして③全身状態改善最優先（特に高血糖）を考え，利益と不利益の主観的評価は図に示すように想定した．図で斜線（＝利益の期待値）が格子（不利益の期待値）を凌駕する度合いの大きいのは，②抗精神病薬投与らしいとわかる．計算でも，図の説明の

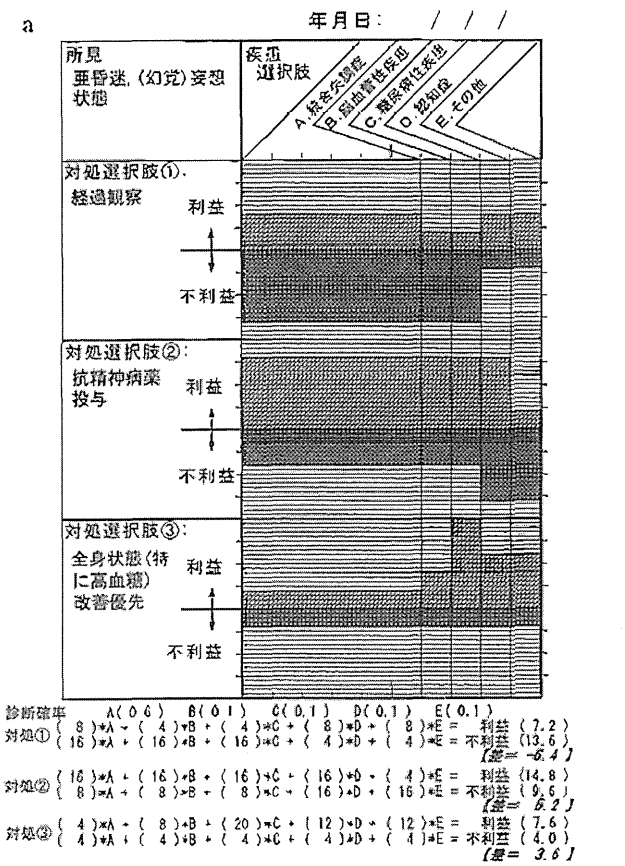


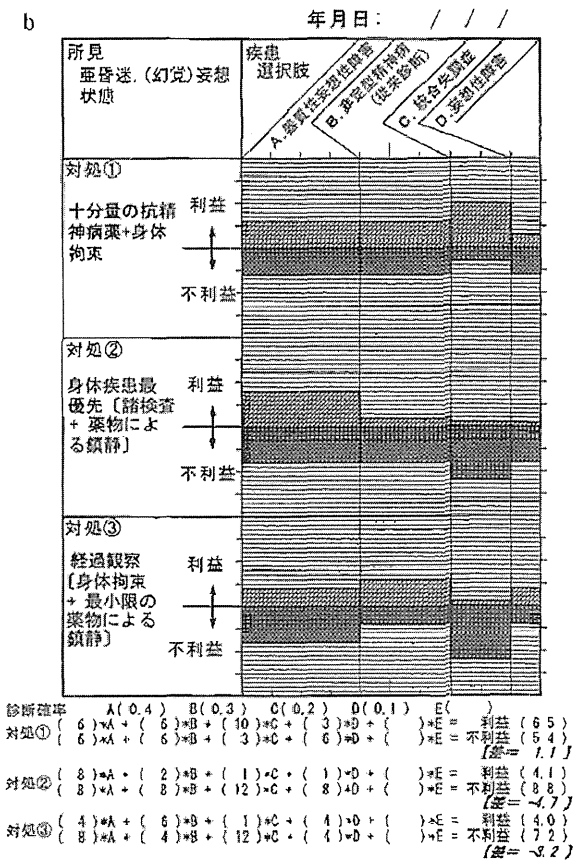


図2

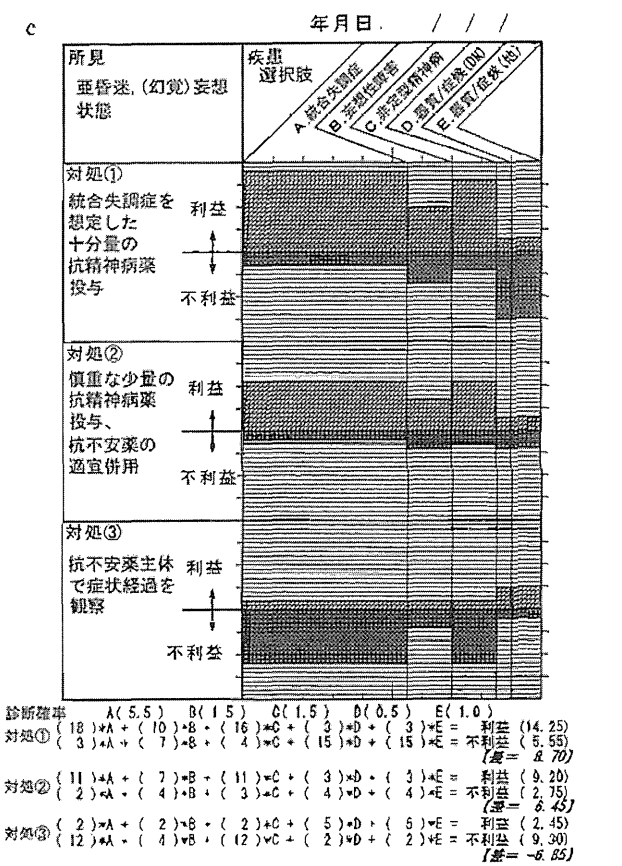


とおり，そのことが裏付けられる．

ただし指導医は，グループ内での討論において，統合失調症の可能性を大きく考えることは当然で既知のことと捉えていたようで，むしろ脳器質性・症状性疾患を見逃すことの重大性について強調して発言していた．

研修医の記入結果は指導医とかなり違っていた．疾患選択肢として，A. 器質性妄想性障害，B. 非定型精神病〔従来診断の〕，C. 統合失調症〔妄想型〕，D. 妄想性障害の4つを考え，主観的確率は，0.4，0.3，0.2，0.1とした．対処選択肢として，①十分量の抗精神病薬＋隔離拘束，②身体疾患最優先〔諸検査＋薬物による鎮静〕，③経過観察〔隔離拘束＋最小限の薬物による鎮静〕を考え，その利益と不利益は図2bのように評価した．図から，選ぶべき選択肢は①と思われ，計算でもそのことが裏付けられる．

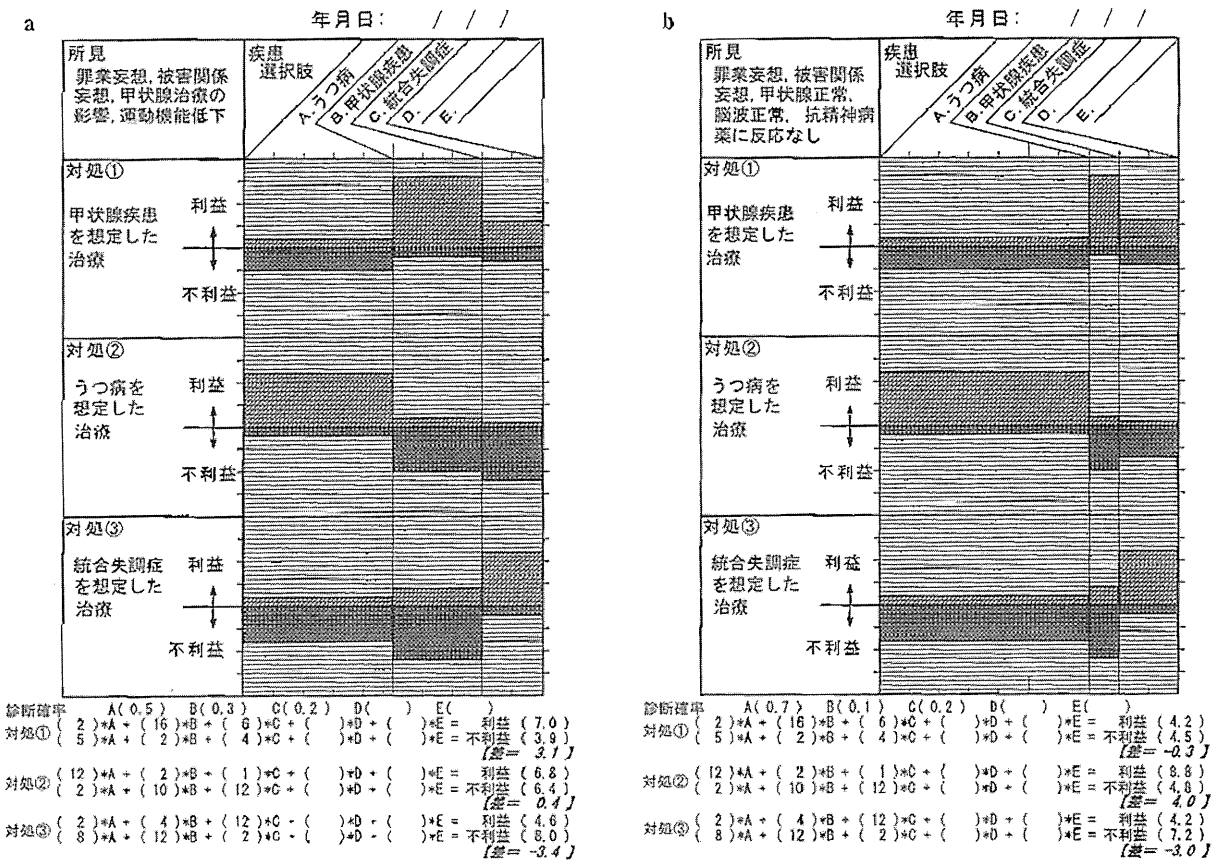


図3

回診医の考えは，どちらかと言えば指導医に近かった．暫定的な疾患選択肢として，A. 統合失調症〔遅発性パラフレニアを含む〕，B. 妄想性障害，C. 非定型精神病〔従来診断の〕，D. 脳器質性・症候性疾患〔糖尿病関連〕，E. 脳器質性・症候性疾患〔糖尿病以外〕の5つを考え，対処選択肢としては①統合失調症を想定した十分量の抗精神病薬，②慎重な比較的少量の抗精神病薬（場合により気分安定薬なども併用），③抗不安薬主体で経過観察の3つを想定した．疾患と対処に関する評価は視覚的・直感的に紙上で検討し，図2cのようにした．選択する対処選択肢は図からも計算上も①十分量の抗精神病薬となる．

3-2. 縦断的評価：1名による複数回評価

【症例3】48歳の女性．某年3月某日入院．

〈入院当日〉

本例の評価図を図3aに示す．

入院時の所見をまとめると，

- 罪業妄想，被害・関係妄想，自殺念慮．病識なし．
- 甲状腺疾患の治療後に精神科の服薬を中断，それに一致して悪化したらしい．
- 半身の「運動機能低下」の訴えあり．
- 体動の遅鈍化傾向．

主治医は，疾患選択肢として，A. うつ病，B. 甲状腺関連の症状精神病，そしてC. 統合失調症の3つを考え，対処選択肢として，①症状精神病を想定した対処〔＝甲状腺を含めた症候性・器質性疾患の徹底した検査，比較的少量の抗精神病薬〕，②うつ病を想定した対処〔＝抗うつ剤をしっかりと使用，一般的レベルの身体的検査〕，そして③統合失調症を想定した対処〔＝抗精神病薬をしっかりと使用，一般的レベルの身体的検査〕を考えた．各疾患選択肢および対処選択肢の主観

的確率は図のとおりである（根拠は省略）．

図から，利益が不利益を凌駕する度合いの最も高い対処選択肢，すなわち斜線が格子を凌駕する度合いが最も大きいのは「①症状精神病を想定した対処」らしいことがわかる．念のため面積を計算すると，①②③の実質利益期待値はそれぞれ3.1，0.4，−3.4となり，そのことが裏付けられる．

〈5日後〉

5日後時点の評価図を図3bに示す．

若干の追加情報が得られた．

・バセドウ氏病だが，現在機能障害なし．

・脳波では異常なし．

・抗精神病薬数日使用で反応に乏しい．

これに基づいて，主治医は，症状精神病の確率を下げ，その分をうつ病に回し，主観的確率を0.7，0.1，0.2に変更した．

図から，利益が不利益を凌駕する度合いの最も高いのは，初回と違い，「②うつ病を想定した対処」となっている．計算でも，図の説明のように，①②③の実質利益期待値はそれぞれ−0.3，4.0，−3.0となり，②の選択が妥当であることが裏付けられる．

## III. 考　　察

以上，不完全情報下での診療状況の諸要因をわかりやすく提示する工夫について述べた．目的は，自身の診療上の意思決定，他医師とのコミュニケーション，患者や家族への説明などに役立てることであった．この評価図を使うに当たって最も重要なのは，何度も言及したように，頭の中の判断過程を視覚的に出力することである．数値計算用データがあればそれに越したことはないが，描き出して，それをもとに説明や議論といった活動に役立てることが第1の目的である．

本稿では方法の記述に重点を置いたため，試用者の感想などに関する記述は割愛した．今後まとまった数の施行を行って有用性を検討する必要があろう．ここでは，今回取り上げた症例の担当医をはじめ，過去に試用を依頼した研修医や指導医には概ね好評であったこと，意外にも理解困難を訴える者がいなかったこと，などを述べるに止めたい．

この方法は，十分な情報を集め，診断を確定し，エビデンスに基づいた治療を行うという一般的方法を否定するものではない．むしろ著者の意図は，現在の精神医学の不完全性とそれに由来する不完全情報下での診療状況（特に入院初期や初診時）を直視し，一般的方法が通用しない部分を補完しようというものである．このことは確認しておきたい．

ところで，我が国では昨今，診療報酬の包括支払い方式が次第に一般的となりつつある．精神科は従来その対象から外されていたが，今後は対象に含まれる可能性がある．その際，大きな問題になると思われるのは，診断と治療との対応の問題である．身体疾患では，「まず診断を確定し，その診断に対応する評価・治療セットを選択する」という行き方が有用であろう．しかし，病因の不明な疾患が大半を占める精神科においては，診断基準という約束事を持ち込むことで形式的には確定診断は得られるが，それはあくまでも約束事であって，自然現象そのものではない．つまり，確定診断とはいっても，それはいわば仮の確定診断である[8]．したがって，上記のような身体疾患のモデルをそのまま持ち込むことは，肝心の治療効果の最適化を阻害する危険性がある．対応を若干緩く考えたうえで結果を観察しながら試行錯誤と微調整を行うという方針の方が，最適化に至る可能性は高いのである．経験のある精神科医は，このことを理解できる．しかし，他科の医師や医師以外の職種の人にはこうした精神科の特殊性は理解されにくい．本稿の図示法が，現段階の精神医学のこうした不確定性という側面を意識化する意味で，包括支払い方式に伴う精神科治療の画一化の防止にも役立つことを期待したい．

本稿で示した評価図には，いくつかの重大な限界がある．

最大の限界は，確率計算[1,2,5,6]のためのデータベースが不足していることである．本稿では，個

人経験に基づく主観的な印象をそのまま図示する方法をとった．現段階で我々の日常的診療が，ある程度はデータに準拠しつつも，かなりの部分個人的経験を取り入れざるを得ないのが実態である以上，こうした方法には，十分に意味がある．実際，過去にも主観的確率を診療に取り入れるための方法は報告されている[3,4]．しかし，客観的データベースが使えるのであれば，それに越したことはない．今後，各診断の出現率や各診断中の主な所見の出現率などの基本データの蓄積が望まれる．

もうひとつの限界は，疾患分類システムの問題である．すでに指摘したように，現在の疾患分類システムは概ねよく検討されたものであり，実際に広く使われている．しかし，意思決定の枠組みに用いるには不十分な点がある．意思決定のためには，各疾患の概念は治療反応性や経過などの時間縦断的特性をより十分に含む必要がある．また，経過を追ううちに他の診断に移行するような暫定的分類や煩雑な細分類は撤廃して診断単位をより大きくまとめ，それらは，DSM-IVの気分障害の“specifiers”のように，疾患内部のバリエーションとする方が実際的であろう[7]．今後，臨床的意思決定の枠組みに適した，より実際的な疾患分類の出現が望まれる．

## 文　献


1) 福井次矢：臨床医の決断と心理．医学書院，東京，1988

2) 古川壽亮，神庭重信編：精神科診察診断学―エビデンスからナラティブへ―．医学書院，東京，2003

3) Giovanni, P.: Modeling in medical decision making: a Bayesian approach. John Wiley & Sons, Ltd, 2002

4) Gustafson, D.H., Sainfort, F., Johnson, S.W., et al.: Measuring quality of care in psychiatric emergencies: construction and evaluation of a Bayesian Index. Health Service Research, 28; 131-158, 1993

5) 森田優三：意思決定の統計学（講談社現代新書）．講談社，東京，1971

6) 太田敏男，山内俊雄：意思決定問題としてみた精神科診療の構造について．精神科診断学，6；45-46，1995

7) 太田敏男：精神科における「意思決定問題の枠組み」の重要性について．精神経誌，102；1015-1029，2000

8) 太田敏男：「ベクトル診断」の紹介―伝統的診断方法の定式化の観点から．精神医学，48；529-537，2006

9) Spitzer, R.L., Endicott, J., Robins, E.: Clinical criteria for psychiatric diagnosis and DSM-III. Am J Psychiatry, 132; 1187-1192, 1975

技術講座　生理

# 光トポグラフィー検査(NIRS)による脳機能測定

福田正人　吉田寿美子　杉村有司　小川　勝
大渓俊幸　樋口智江　内山智恵　安井臣子

検査と技術
第40巻　第3号　別刷
2012年3月1日　発行

医学書院

# 光トポグラフィー検査(NIRS)による脳機能測定

福田正人[*1]・吉田寿美子[*2]・杉村有司[*2]
小川 勝[*3]・大渓俊幸[*4]・樋口智江[*4]
内山智恵[*4]・安井臣子[*4]

## 新しい知見

“光トポグラフィー”は，近赤外線(光)を用いて脳機能を検査する近赤外線(光)スペクトロスコピー(near-infrared spectroscopy，NIRS)の保険収載名である．2002年より脳外科手術前の検査として保険適用となっていたが，2009年に精神疾患における「うつ症状の鑑別診断補助」として先進医療の承認を受け，精神疾患についての初めての臨床検査となった．精神疾患は，受診患者が300万人を超え，厚生労働省により医療法に基づく5大疾病の一つに定められたので，今後は検査希望が増えるものと予想される．

## 用語解説

●近赤外線(光)…赤の可視光と遠赤外線(光)の中間の光．生体をある程度は透過し，ヘモグロビンにより吸収されやすい特徴があるため，生体のヘモグロビン濃度の測定に利用できる．パルスオキシメータは指についてその透過光を利用することで，動脈血の酸素飽和度を測定している．

●近赤外線(光)スペクトロスコピー(NIRS)…近赤外線を用いて生体のヘモグロビン濃度を計測し，局所の血液量を推定する方法論．“近赤外分光法”とも呼ばれる．頭部について散乱光を利用すると，頭表から2～3 cmの範囲が測定でき，大脳皮質の血液量変化を捉えることができる．そのデータは，脳活動に伴う大脳皮質の活性化を反映する．

●光トポグラフィー…頭部用のNIRSによる脳機能測定についての保険収載検査名．所要時間や手技の点で，脳波より簡便な検査である．

●先進医療…厚生労働省が「将来的な保険導入のための評価を行うために，保険給付の対象とすべきものであるか否かについて，適正な医療の効率的な提供を図る観点から評価を行うことが必要」と定める医療．新規治療薬の臨床治験に相当し，研究から診療への発展を検討するための中間段階と位置づけられる．

●うつ症状…精神疾患の症状として認められる，うつと関連する気分や行動や身体についての症状．うつ病に限らず，双極性障害(躁うつ病)・統合失調症など他の精神疾患においても広く認められるため，原因となる疾患についての鑑別診断が必要となる．

[*1] 群馬大学大学院医学系研究科神経精神医学・准教授 〒371-8511 前橋市昭和町3-39-22
[*2] 国立精神・神経医療研究センター病院臨床検査部 [*3] 国立病院機構沼田病院臨床検査部
[*4] 東京都立松沢病院検査科


0301-2611/12/¥250/論文/JCOPY